The Astrophysical Journal, 725:1485–1494, 2010 December 20 doi:10.1088/0004-637X/725/2/1485

THE FORMATION OF LOW-MASS BINARY STAR SYSTEMS VIA TURBULENT FRAGMENTATION

Stella S. R. Offner[1], Kaitlin M. Kratter[2,3], Christopher D. Matzner[2], Mark R. Krumholz[4], and Richard I. Klein[5,6]
[1] Harvard-Smithsonian Center for Astrophysics, 60 Garden Street, Cambridge, MA 02138, USA; soffner@cfa.harvard.edu
[2] Department of Astronomy and Astrophysics, 50 St. George Street, University of Toronto, Toronto, Ontario M5R 3H4, Canada
[3] Institute for Theory and Computation, Harvard-Smithsonian Center for Astrophysics, 60 Garden Street, Cambridge, MA 02138, USA
[4] Department of Astronomy and Astrophysics, University of California, Santa Cruz, CA 95064, USA
[5] Department of Astronomy, University of California, Berkeley, CA 94720, USA
[6] Lawrence Livermore National Laboratory, Livermore, CA 94550, USA
Received 2010 July 2; accepted 2010 October 16; published 2010 November 29

ABSTRACT

We characterize the infall rate onto protostellar systems forming in self-gravitating radiation-hydrodynamics simulations. Using two dimensionless parameters to determine the disks' susceptibility to gravitational fragmentation, we infer limits on protostellar system multiplicity and the mechanism of binary formation. We show that these parameters give robust predictions even in the case of marginally resolved protostellar disks. We find that protostellar systems with radiation feedback predominately form binaries via turbulent fragmentation, not disk instability, and predict that turbulent fragmentation is the dominant channel for binary formation for low-mass stars. We clearly demonstrate that systems forming in simulations including radiative feedback have fundamentally different parameters than those in purely hydrodynamics simulations.

Key words: accretion, accretion disks – binaries: general – radiative transfer – turbulence

Online-only material: color figures

1. INTRODUCTION

The study of stellar multiplicity is a centuries-old pursuit (Mitchell 1767), yet we still lack a comprehensive theory explaining the formation of the wide range of observed binaries and multiple systems. In this paper, we investigate the relative importance of two paths for binary formation using simulations of a turbulent molecular cloud destined to form a small cluster of low-mass stars.

Although there are numerous proposed mechanisms for binary formation (see, for example, Tohline 2002), we focus here on two prominent channels: the fragmentation of a turbulent core and the fragmentation of a gravitationally unstable disk. Briefly, the turbulent core hypothesis (Goodwin et al. 2004; Fisher 2004) posits that turbulent fluctuations within a bound core can produce multiple nonlinear perturbations in density, which exceed the local Jeans mass and collapse faster than the background core. Multiple peaks within a given core result in a bound binary or multiple stellar system.

The second hypothesis, disk fragmentation (Adams et al. 1989; Bonnell & Bate 1994), suggests that disks subject to sufficiently strong gravitational instability might fragment to form one or more companions. Although previous studies suggested that this process was limited to large mass ratio systems, recent work such as Stamatellos & Whitworth (2009) and Kratter et al. (2010a) has shown that when disks continue to be fed at their outer edges, the companions can grow substantially.

The latter process has shown promise in its application to high-mass stars (Kratter & Matzner 2006; Krumholz et al. 2007), where rapid mass accretion pushes disks toward instability. One of the goals of this paper is to investigate whether the conditions in low-mass turbulent cores are ever sufficiently violent to induce disk fragmentation.

Observations offer limited guidance as to which mechanism dominates, although several lines of evidence indicate that turbulent fragmentation must account for at least some of the binary population. At wide separations, binaries show a very broad eccentricity distribution (Melo et al. 2001) and random orientations between the binary orbital plane and the spins of the component stars (Hale 1994). Similarly, disks around wide T Tauri star binaries show significant misalignment between the planes of the disks and the binary orbit (Jensen et al. 2004; Monin et al. 2006; Scholz et al. 2010). High eccentricity and orbital misalignment are inconsistent with these binaries having been created via the fragmentation of a single planar disk (unless they result from three-body interactions) but are expected from turbulent fragmentation. In contrast, binaries at small separations have reduced eccentricities and far less misalignment between the orbital plane and the spin or disk orientations of the individual components. However, this can plausibly be explained via tidal circularization of initially misaligned systems (e.g., Lubow & Ogilvie 2000; Bate et al. 2000), so these binaries may have formed by either turbulent or disk fragmentation. Moreover, misalignment of the spin–orbital plane of systems born in disks may also be due to n-body interactions and ejections in a multiple system. Consequently, observations are at present unable to answer the question of whether disk fragmentation can be responsible for a significant fraction of binaries. (See Howe & Clarke 2009 for a further discussion of the observational evidence on this point.)

Previous analytic work (Matzner & Levin 2005) and numerical studies of isolated disks have suggested that disks around low-mass stars will be stable (Boley et al. 2007; Cai et al. 2008). This work has shown that appropriate thermal treatment is essential, and in particular that heating by the central star dominates at distances beyond tens of AU. Recent numerical simulations of low-mass star formation have demonstrated that small-scale

fragmentation leading to high-multiplicity systems is indeed reduced when radiative feedback is included (Offner et al. 2009b; Bate 2009).[7]

Despite these advances, resolving both the large-scale turbulence of a molecular cloud forming an ensemble of stars and the details of disk structure remains computationally challenging. In order to resolve the opacity limit for fragmentation, smoothed particle hydrodynamics methods require mass resolution of $10^{-2}\,M_{\odot}$, while grid-based methods must achieve resolutions down to a few AU (Goodwin et al. 2007). Simulations often circumvent this difficulty by modeling individual dense cores with simple initial conditions (e.g., Klessen & Burkert 2000; Goodwin et al. 2004; Walch et al. 2009). Such work is predicated on the knowledge of isolated core properties and sacrifices the interaction of cores with their turbulent environment (Offner et al. 2008).

In this paper, we examine the simulations of Offner et al. (2009b, hereafter OKMK09), which follow the birth and evolution of protostars in a turbulent molecular cloud, in light of the criteria for protostellar disk fragmentation recently proposed by Kratter et al. (2010, hereafter KMKK10). We do this with the goal of drawing conclusions about aspects of stellar binary formation which are not resolved within OKMK09. We proceed in two steps: first we test the KMKK10 stability criteria against non-isothermal, turbulent simulations using the high-resolution runs from OKMK09 and then we apply these criteria in order to predict the outcome of under-resolved disk accretion in the low-resolution OKMK09 simulations. Ultimately, we can assess the relative importance of turbulence and disk instability in the creation of low-mass stellar binaries.

In the following sections we define our key dimensionless parameters, outline our testing scheme, describe our numerical methodology, and ultimately draw conclusions about the nature of low-mass star formation.

2. CHARACTERIZING ACCRETION AND DISK FRAGMENTATION

2.1. Dimensionless Parameters

Classically, disks are thought to fragment and become unstable when self-gravity becomes sufficiently strong as measured by a low value of Toomre's Q parameter:

$$Q = \frac{c_{\rm s,d}\Omega_{\rm d}}{\pi G \Sigma_{\rm d}}, \tag{1}$$

where $\Omega_{\rm d}$ is the disk angular velocity, $\Sigma_{\rm d}$ is the disk surface density, and $c_{\rm s,d}$ is the disk sound speed (Toomre 1964). More recent work has shown that disk gas must also be able to cool efficiently once the process of collapse begins in order to fragment (Gammie 2001). The latter criterion is a strong constraint in the inner parts of disks where viscous heating dominates but is typically satisfied in the outer radii of the irradiated disks that we study here (Kratter et al. 2008, 2010b).

Although Q remains a good predictor of disk fragmentation, it is of more limited use for evaluating disk stability in both large-scale star formation simulations and observations because it requires precise knowledge of local disk properties, which are difficult to model and measure.

[7] Bate (2009) includes radiative transfer on numerically resolved scales, but not radiation feedback from nuclear or accretion luminosity of stars, which Offner et al. (2009) show is roughly an order of magnitude larger. In that respect, Bate's simulations represent an intermediate case between non-radiative and radiative simulations.

Young protostellar disks are typically driven unstable only when they receive mass faster than they can process it down onto the central star (Matzner & Levin 2005). Thus, it is useful to parameterize disk fragmentation as a function of the infall rate from large scales. KMKK10 demonstrated that one can predict disk fragmentation under idealized conditions using two dimensionless numbers normalized to the infall rate. One, the thermal parameter ξ, compares the disk sound speed to the mass accretion rate:

$$\xi = \frac{\dot{M}_{\rm in} G}{c_{\rm s,d}^3}, \tag{2}$$

where $\dot{M}_{\rm in}$ is the infall mass accretion rate. This relates to the Shakura & Sunyaev (1973) α parameter through $\xi = 3\alpha/Q$. Increasing ξ at fixed α tends to cause Q to decrease until self-gravity becomes strong ($Q \sim 1$), at which point gravitationally induced spiral modes lead to an increase in the effective value of α. Beyond critical values of ξ and α, however, the disk will fragment; practically this occurs when $\xi \simeq 2$ and $\alpha \simeq 2/3$. For instance, a strictly isothermal simulation fed by a slowly rotating Shu (1977) solution, in which $\xi = 0.975$, should show strong spiral arms but not fragment, whereas one fed by the Foster & Chevalier (1993) collapse solution, in which $\xi \gg 1$ at early times, should fragment.

A second parameter, Γ, measures rotation by comparing the orbital period of the infalling gas to the accretion timescale:

$$\Gamma = \frac{\dot{M}_{\rm in}}{M_{*\rm d}\Omega_{\rm k,in}} = \frac{\dot{M}_{\rm in}\langle j\rangle_{\rm in}^3}{G^2 M_{*\rm d}^3}, \tag{3}$$

where $M_{*\rm d}$ is the total mass in the star–disk system, $\Omega_{\rm k,in}$ is the Keplerian angular velocity at the circularization radius of the infall, and $\langle j\rangle_{\rm in}$ is the average specific angular momentum. A large value of Γ, e.g., 10^{-1}, implies that the system mass changes significantly in only a few disk orbits, whereas small values, $\Gamma \sim 10^{-4}$ to 10^{-3}, describe disks with a mass doubling time of hundreds to thousands of orbits. The magnitude of Γ affects the disk's aspect ratio ($H/R_{\rm d} \simeq (\Gamma/\xi)^{1/3}$), and therefore the winding of spiral arms, and the mass of forming fragments.

Conducting idealized collapse experiments with ORION, a three-dimensional (3D) Adaptive Mesh Refinement (AMR) gravito-radiation-hydrodynamics code, KMKK10 probed the fragmentation threshold and final outcome (single, binary, or multiple) for isothermal disks in which ξ and Γ are constant but numerical resolution improves over time. They concluded that any disk with $\xi > 2$–3 will fragment, for values of Γ typical of low-mass star formation ($10^{-3} \lesssim \Gamma \lesssim 10^{-2}$), and that increasing Γ has a weak stabilizing effect.

KMKK10 argued that ξ and Γ capture the essential aspects of disk thermodynamics in the context of steady accretion and that other parameters, such as the cooling time compared to $\Omega_{\rm k,in}^{-1}$, influence fragmentation only through their effect on ξ. This assertion is not tested within their isothermal simulations, but in Section 4 we confirm that it is consistent with the behavior of our highest resolution (non-isothermal) runs. We then treat ξ and Γ as robust predictors of unresolved disk instability and fragmentation in our lower resolution simulations.

3. METHODS

3.1. Numerical Methodology

In this section, we give a brief overview of the simulations completed in OKMK09 that are the basis for this work. The

calculations are performed with the ORION AMR code. The simulation boxes have initially uniform density and periodic boundary conditions. Energy is injected in the form of small velocity perturbations with wave numbers in the range $1 \leqslant k \leqslant 2$ for three crossing times until a turbulent steady state is achieved. The calculation we refer to as RT includes radiative transfer in the flux-limited diffusion approximation, while the second calculation, NRT, uses a barotropic equation of state (EOS) that has no mechanism for the transport of radiation. Since radiative cooling is very efficient during the initial driving phase, all of the gas remains close to 10 K in the RT run, and both calculations begin with a similar temperature.

After three crossing times, self-gravity is turned on and this point is considered $t = 0$. The initial mean density is 4.46×10^{-20} g cm^{-3}, the 3D Mach number is 6.6, and the total mass is 185 $M_{\odot}$. Energy continues to be injected at a constant rate to offset the natural turbulent decay throughout the run (e.g., Stone et al. 1998). Stars are inserted as point particles once the Jeans criterion is exceeded on the maximum level (Krumholz et al. 2004). In the RT calculation, the stars are endowed with a subgrid stellar evolution model, which includes accretion luminosity down to the stellar surface, Kelvin–Helmholtz contraction, and nuclear burning (see OKMK09 for a detailed description). The calculations evolve with gravity for one cloud free-fall time or 0.315 Myr.

The RT and NRT runs have a minimum AMR cell size of 32 AU such that protostellar disks are only marginally resolved with ∼10 cells. Although the simulations refine based upon the Jeans length, thus preventing artificial fragmentation (Truelove et al. 1997), they do not resolve the disk scale height with more than a few cells (Nelson 2006). Nonetheless, OKMK09 demonstrated that the protostellar accretion rates are converged to within a factor of 2 by running a resolution study of the first forming protostar in each with an extra three levels of AMR refinement and minimum cell spacing of ∼4 AU. We use the high-resolution studies RTC and NRTC to assess convergence.

3.2. Data Analysis

Our parameterization in terms of ξ and Γ requires that we distinguish disk matter from the infall, so that we can evaluate the disk sound speed $c_{\rm s,d}$ and the angular momentum scale $\langle j \rangle_{\rm in}$ in addition to the accretion rate $\dot{M}_{\rm in}$. The first step is to define the disk-accretion boundary in a robust way within our simulations. Imposing a density cutoff is not sufficient as the protostellar cores have a range of conditions which produce diverse disk properties. Automatic identification is complicated by disk flaring, close companions, and turbulent filaments of gas feeding the disks. For the RT and NRT calculations, we adopt a relatively low-density threshold of 10^{-16} g cm^{-3}. We estimate the total angular momentum vector of the gas and rotate the coordinate frame so that the net angular momentum vector is parallel to the z-axis. Finally, we restrict the vertical disk height in the z direction to ± 5 cells from the disk midplane. The combination of a gas density cut with these geometric constraints captures the flaring and warping of the disk, while excluding gas flowing into the disk. These criteria are not sufficient to remove abutting disks of very nearby companions from the sample, but these events are few and are easily identified from changes in the estimate of the disk radius. In the case of a multiple system with a single disk, we perform the analysis in the reference frame of the primary.

Once the disk material is identified, we estimate the disk mass, radius, mean temperature, accretion rate, and angular momentum. The disk radius, $r_{\rm d}$, is defined by the distance between the farthest disk cell and the protostellar location. The mean sound speed, $c_{\rm s,d}$, is given by $\sqrt{k_{\rm B} T_{\rm d}/\mu_{\rm p}}$, where $\mu_{\rm p} = 2.33\, m_{\rm H}$ is the mean particle mass and $T_{\rm d}$ is the mean mass-weighted temperature averaged over the disk. We find that constructing a volume-weighted mean changes the resulting temperature by at most 15%. The accretion rate, $\dot{M}_{\rm in}$, is calculated by taking the difference between the total star–disk system mass, $M_{*\rm d}$, from one time step to the next. In rare cases, $\dot{M}_{\rm in}$ may be negative if the disk is perturbed by a nearby companion or passes through a shock.

We find that varying the density threshold by factors of 2 has a 10%–15% effect on the disk mass and accretion rate but may translate into a 50% difference in Γ and ξ, since these parameters are implicitly sensitive to the disk radius and the amount of included or excluded high angular momentum material near the disk boundary. The RTC and NRTC runs, which have better resolved disk structure and sharper disk edges, serve as limits on the sensitivity to specific disk properties. We discuss in more detail in Section 5.1 how the parameters change when defined on larger scales.

4. RESULTS

4.1. Final Protostellar System Outcomes

Figure 1 shows examples of several systems formed in each of the runs (RT, NRT, RTC, and NRTC). The systems can be divided into three classes: isolated stars, binaries and multiples formed via the fragmentation of a turbulent core, and binaries and multiples formed via the fragmentation of a disk. Because disk radii are of order a few hundred AU, whereas turbulent fragmentation of a core can occur on scales up to the Bonnor–Ebert radius (0.05 pc = 10^4 AU for $n_{\rm H} = 10^5$ cm^{-3}, $T = 10$ K), we use 500 AU as a crude dividing line.

In Figure 2, we show the separation of all possible pairs of stars, bound or unbound, as a function of time in the simulations including radiative feedback (RT). All but one binary system form outside of 500 AU, but within a typical core radius. Upon inspection, the exception results not from disk fragmentation but rather from fragmentation of a cold filament or stream feeding a more massive protostar. We conclude that fragmentation leading to binaries in the RT run is consistent with core, not disk, fragmentation.

Note that the pairs that appear to diverge in Figure 2 are unaffiliated stars, not spreading binaries. Pairs with separations greater than 0.1 pc are excluded since they clearly form in different cores and cannot result from turbulent core fragmentation.

The fragmentation history in the calculations without feedback is quite different. Turbulent fragmentation still occurs on core scales, but now protostellar disks also fragment; see Figure 1. As discussed in OKMK09, and as predicted by Matzner & Levin (2005), this additional fragmentation would have been suppressed by realistic heating of the disk via radiative feedback. In run NRT, which lacks such heating, disk fragmentation leads to several large multiple systems and the dynamical ejection of a few of the smaller companions. Considering that radiative feedback is present in low-mass star formation, we conclude that turbulent core fragmentation is likely responsible for the low-mass stellar binary population.

4.2. Simulation Thermal and Rotational Parameters: ξ and Γ

We find that the thermal parameter, ξ, as illustrated in Figure 3 is either constant or decreasing with time for each

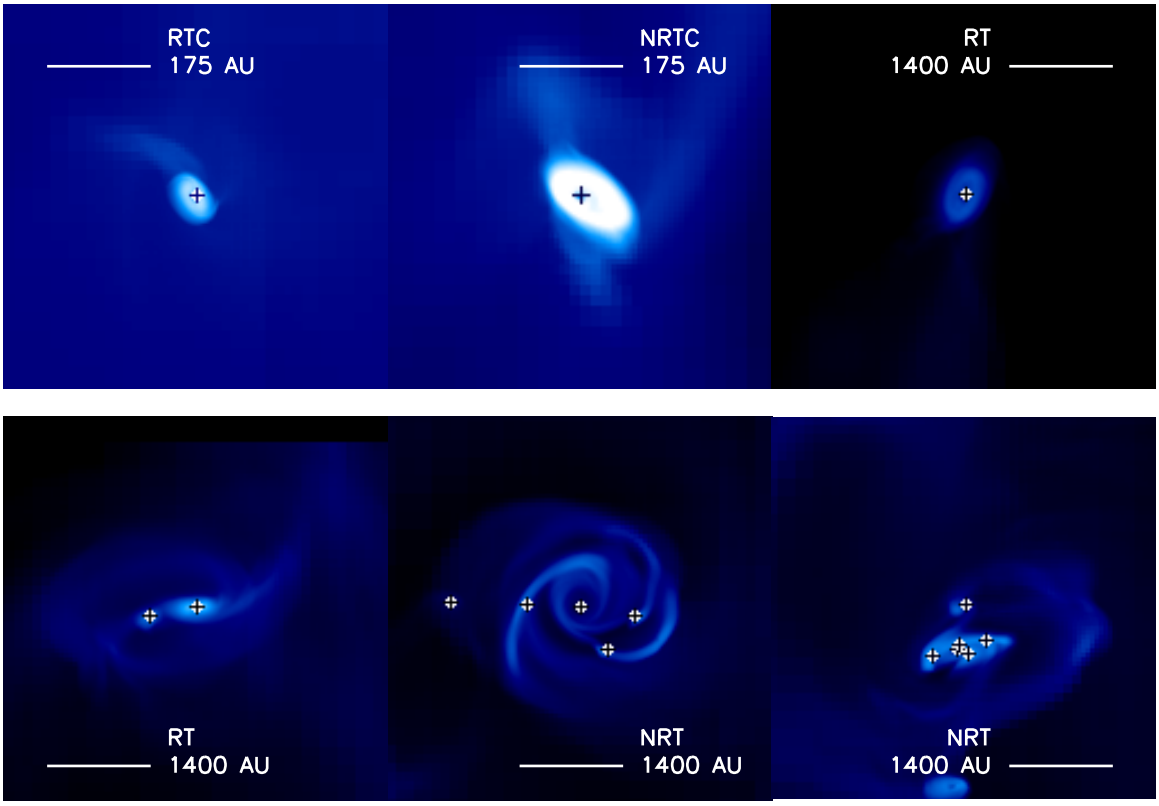

Figure 1. Log gas column density for six different protostellar systems, where the star positions are marked by crosses. The column density scale runs from 0.1 g cm^{-2} to 100 g cm^{-2}. The scales of the image and run are indicated.

(A color version of this figure is available in the online journal.)

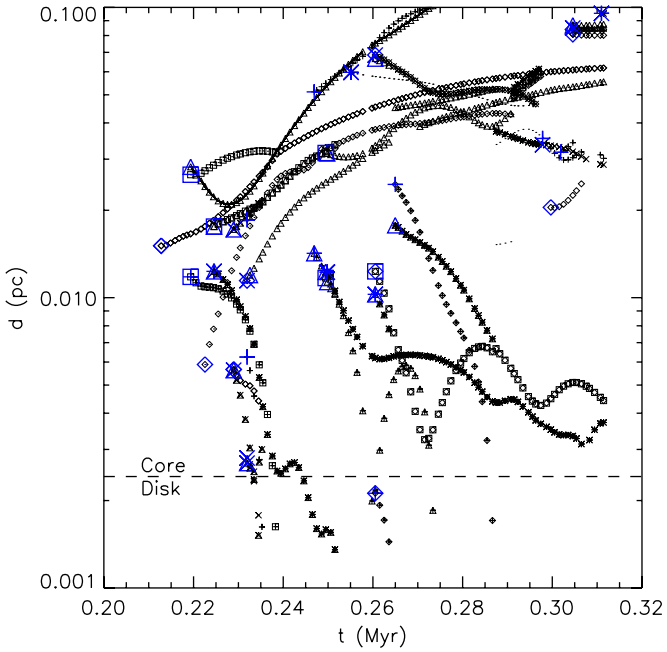

Figure 2. Pair separation as a function of time in 1 kyr bins for pairs in the RT simulation, where each symbol indicates a different pair. The dashed line at 500 AU indicates a rough boundary between the disk and core scale, where the mean disk size in the RT simulation is approximately 500 AU. The large majority of pairs have separations above 0.1 pc and are not shown here. The large (blue) symbols indicate the first time bin.

(A color version of this figure is available in the online journal.)

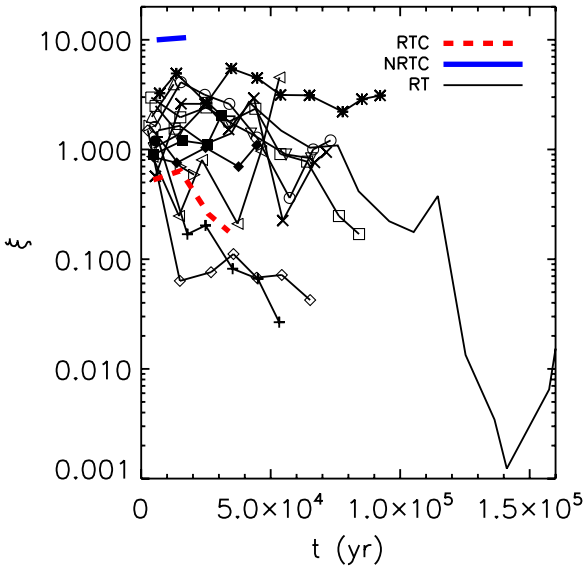

Figure 3. Thermal parameter, ξ, as a function of time for the protostellar disks in each simulation. The high-resolution RTC (dashed, red) and NRTC (solid, blue) runs are shown in bold. The solid line without a symbol corresponds to the same first forming star that is depicted by the RTC and NRTC runs. The data are averaged over 10^4 yr bins.

(A color version of this figure is available in the online journal.)

system. As shown, most protostars begin with mean values of ∼1–3, skirting the regime where fragmentation is possible.

The decline in ξ over time primarily reflects that the accretion rates decrease as the disk temperatures do not increase significantly. This is consistent with observations that the mean accretion rate falls as protostars transition from the Class 0 to Class II stages (Andre & Montmerle 1994; Evans et al. 2009).

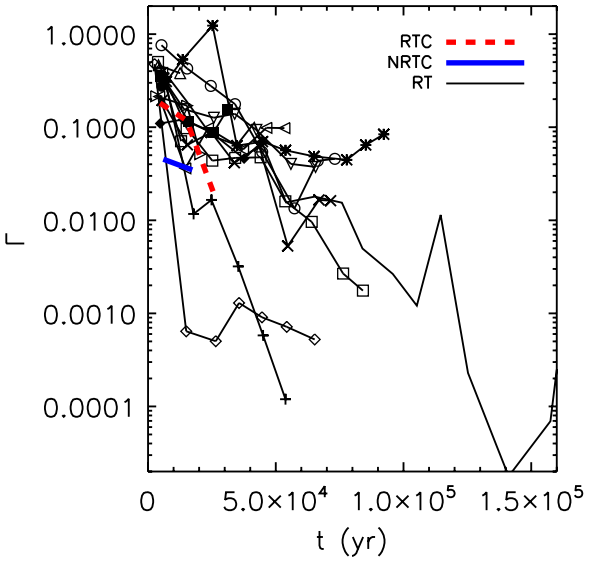

Figure 4. Rotational parameter, Γ, as a function of time for the protostellar disks in each simulation. The lines, symbols, and data bins are the same as in Figure 3.

(A color version of this figure is available in the online journal.)

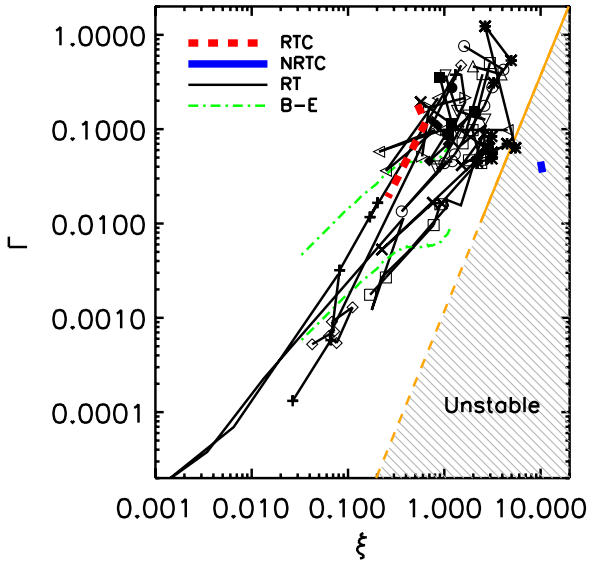

Figure 5. Γ as a function of ξ for the protostellar disks in each simulation. The solid line is the boundary between fragmenting and stable disks found by KMKK10. The dashed line indicates where we have extended it to lower Γ values than explored by KMKK10. Bonnor–Ebert (B–E) spheres for $\beta = 0.08$ (top) and $\beta = 0.02$ (bottom) are given by the (green) dot-dashed lines. The lines, symbols, and data bins are the same as in Figure 3.

(A color version of this figure is available in the online journal.)

By the time protostars reach the Class II stage, their luminosities are dominated by stellar rather than accretion luminosity (White & Hillenbrand 2004).

The ξ value from the NRTC run is shown in Figure 3 for reference. It is apparent that without heating from radiation feedback ξ reaches a value that is a factor of 10 and 20 times larger than its RT and RTC counterparts, respectively. The RTC ξ begins within a factor of 2 of ξ for the corresponding RT protostar. However, the more resolved disk is smaller and has a higher mean temperature so that the values differ by a factor of nearly 10 at 40 kyr. Because $\xi \propto T^{3/2}$, any temperature difference is magnified.

The RT disks cluster around mean temperatures of 30–40 K. Since the protostellar luminosity is comprised of both a stellar and accretion component, heating continues and the disks remain fairly warm even in those cases that the accretion rate, $\dot{M}_{\rm in}$, diminishes to $\simeq 10^{-7}\ M_\odot\ {\rm yr}^{-1}$. In contrast, the disk in the NRTC run, which has a barotropic EOS, remains close to an average temperature of 10 K, a factor of ∼4 smaller than in the cases with radiative feedback.

Figure 4 illustrates that the rotation parameter, Γ, drops rapidly in time. For the first $\sim 10^4$ yr, the decline arises from increasing disk masses, as high angular momentum material settles onto the disk faster than the disk can drain material onto the star.

At later times, decreasing Γ results from declining accretion rates as the core gas is depleted. This trend can be seen in Figure 4 for a number of protostars that have evolved for more than 5×10^4 yr. The NRT and RT Γ values are more similar and fall within the same range of parameter space, because Γ depends primarily on the turbulent initial conditions on large scales, which are mostly unaffected by radiative feedback. Both the Γ and ξ curves exhibit similar shape variation as a function of time due to their linear dependence on the accretion rate.

Figure 5 shows Γ as a function of ξ at different times for the protostellar disks in each simulation. The values fall in a fairly narrow strip of parameter space. Although fluctuations in the variables obscure the trend somewhat, protostars move from the top right of the plot to the bottom left. For comparison, we plot the Γ–ξ tracks for collapsing Bonnor–Ebert spheres, which are initially overdense by 10% (Foster & Chevalier 1993). (We assume that their disks are heated by a factor of 3.5 above the core temperature, consistent with the average of the RT runs.) The Γ values for the Bonnor–Ebert spheres are calculated assuming solid-body rotation with rotational parameters $\beta = 0.02$ and $\beta = 0.08$, where $\beta = E_{\rm rot}/E_{\rm grav}$. Both cases lie within the RT data and mimic the evolution toward lower ξ and Γ with time.

4.3. Test of Fragmentation Criteria

With the ξ and Γ values in hand, we can compare the system outcomes to those predicted by the idealized models of KMKK10. We take advantage of both the NRT and RT runs to explore disk outcomes across the fragmentation boundary in ξ–Γ space. KMKK10 predict systems that fall to the left of the solid line in Figure 5 should be stable to disk fragmentation, while systems to the right should fragment. This is precisely what we find: disks to the right of the line, which are primarily NRT runs, undergo disk fragmentation, while those to the left, primarily RT runs, do not. Note that low resolution often prevents the fragments from surviving to form binaries due to the sink particle algorithm (see Section 5.3); a similar effect was observed in resolution studies in KMKK10. We find that in a few cases, RT disks briefly cross the fragmentation line as a result of short-duration accretion variability.

Figure 6 shows the final values of Γ, ξ, and multiplicity for each protostellar system. Here we define a multiple system as one with bound neighbors within 2000 AU. The RT cases all fall to the left of the fragmentation line, and all binaries in this region are formed via core fragmentation. In contrast, the NRT systems are nearly all to the right of the fragmentation line, with the multiple system having the highest ξ values. Although there are single NRT systems on both sides of the line, we find that those in the fragmenting region have previously or are still experiencing fragmentation and particle merging. The formation

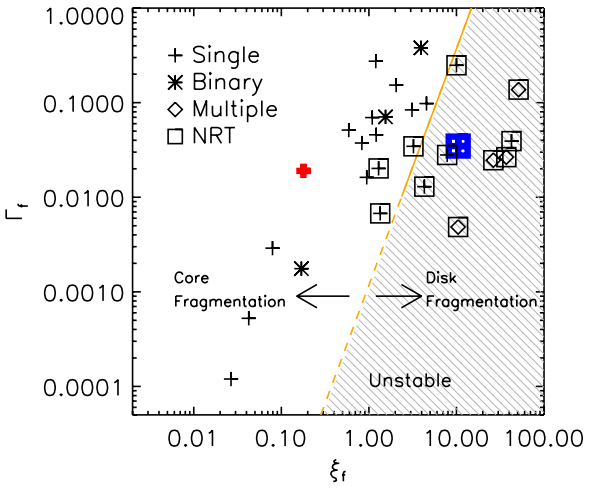

Figure 6. Final values of Γ and ξ at 1 $t_{\rm ff}$ for the protostellar disks in each simulation. The high-resolution RT (red) and NRT (blue) runs are shown in bold. The hatched area indicates ξ and Γ values prone to disk instability as shown in Figure 5.

(A color version of this figure is available in the online journal.)

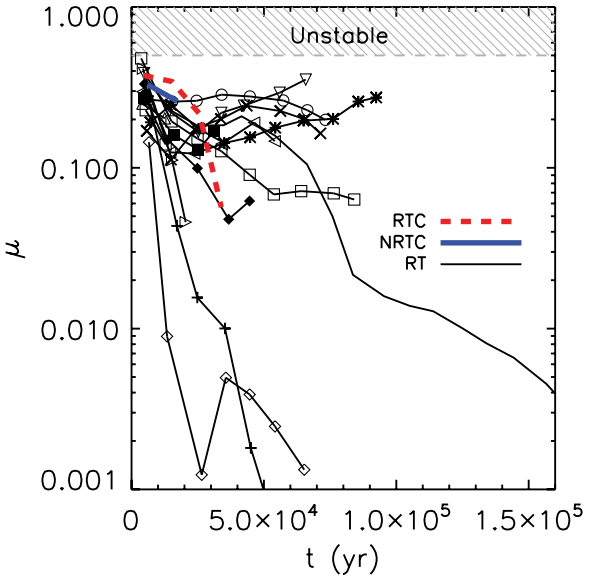

Figure 7. Disk to system mass ratio μ as a function of time for the protostellar disks in each simulation. The lines, symbols, and data bins are the same as in Figure 3. The hatched area indicates values of μ prone to disk instability.

(A color version of this figure is available in the online journal.)

of primarily single systems in the RT run is consistent with the observed multiplicity fraction of low-mass stars (Lada 2006).

4.4. Toomre's Q and Disk to Star Mass Ratios

Although we rely primarily on ξ and Γ to predict disk instability, we also examine both the disk to star mass ratio and Toomre's Q parameter as proxies for disk instability. Following Kratter et al. (2008), we define the ratio of the disk mass to the total system mass as

$$\mu = \frac{M_{\rm d}}{M_{*{\rm d}}}. \quad (4)$$

When the disk and star are of comparable mass, or $\mu \simeq 0.5$, we expect that the disk will be unstable to gravitational fragmentation (e.g., Shu et al. 1990; Kratter et al. 2008). Figure 7 shows μ as a function of time.

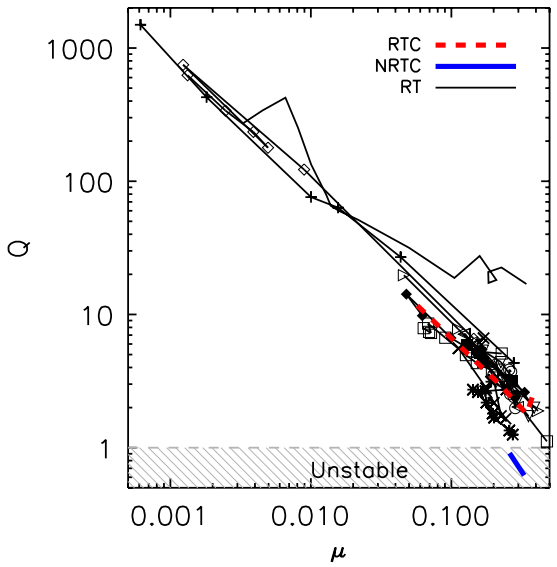

Figure 8. Toomre Q parameter as a function of the ratio of disk to system mass, μ, for the protostellar disks in each simulation. The high-resolution RTC (dashed) and NRTC (solid) runs are shown in bold. The hatched area indicates values of μ and Q prone to disk instability.

(A color version of this figure is available in the online journal.)

To calculate a disk-averaged value for Q, we use the density-weighted temperatures to calculate the disk sound speed. We estimate the disk-averaged surface density as $\Sigma_{\rm d} = M_{\rm d}/(2\pi r_{\rm d}^2)$, where the coefficient 2 assumes a $1/r$ disk column density profile. Because very massive disks ($\mu \sim 0.5$) are especially prone to fragmentation, we show the trajectory of disks in Q–μ space in Figure 8 for the disks in each of the simulations. Thin disks with $Q \lesssim 1$ are unstable to fragmentation. Note that thicker disks fragment at lower values of Q (of order 0.7), while non-axisymmetric gravitational instabilities can set in at $Q \sim 2$ (Goldreich & Lynden-Bell 1965; Sellwood & Carlberg 1984).

At early times, just after the onset of collapse, the protostellar mass is small compared to the disk. However, this phase is brief, approximately a few 10^3 yr, and these structures may in fact be under-resolved flattened envelopes rather than rotationally supported disks. After this early phase, the systems settle into a state where the disk is approximately one quarter of the system mass.

As the core mass is accreted and the protostar grows, μ declines. Both Γ and ξ are positively correlated with the behavior of μ since a declining disk–system ratio signals a declining infall rate.

As suggested by Figure 8, disks in the RT and RTC simulations have $Q > 1$ without exception and thus lie in the stable part of the Q–μ parameter space. In contrast, the NRTC disk approaches $Q \simeq 1$ from below, suggesting that it is extremely unstable at early times. As expected, early fragment formation occurs in the NRTC disk during the first several kyr of the simulation when $Q \simeq 0.7$. As shown in Figure 7, μ generally decreases with time. In Figure 8, declining μ corresponds to larger Q values and increased disk stability.

4.5. Semi-analytic Comparison

Although we measure disk properties directly in these simulations, certain properties remain unresolved at lower resolution and are likely affected by artifacts such as numerical diffusion. In

addition, the previous metrics represent global averages, which may disguise smaller scale instability.

To examine the importance of resolution and global averaging, we make a second estimate of disk stability using simple analytic models to predict radius-dependent disk properties, while still relying on the well resolved infall rates and the luminosities determined in the simulations.

Disks are driven unstable when they are fed material more rapidly than they can process it at a given temperature, i.e., when $\xi \gtrsim 2$, as discussed in Section 2. To evaluate ξ, we estimate disk temperatures at characteristic radii using the disk irradiation models of Matzner & Levin (2005). They find that embedded disks absorb a large fraction of the emitted starlight because the infall envelope is optically thick to visible wavelengths which are caught and re-emitted toward the disk in the infrared. Using a ray-tracing calculation, they find that the flux reaching the disk surface is approximately

$$F_{\rm d} = \frac{f_{*{\rm d}} L_*}{4\pi r_{\rm d}^2}, \tag{5}$$

where

$$f_{*{\rm d}} = 0.11\epsilon^{-0.35} \tag{6}$$

and ϵ is the accretion efficiency from the core onto the star–disk system. We adopt $\epsilon = 1/3$ here (see discussion in Section 5.2). The temperature of a disk in which irradiation dominates over viscous heating, and which is optically thick at all relevant wavelengths, will be

$$T_{\rm d,ir} = \left(\frac{f_* L_*}{4\pi r_{\rm d}^2 \sigma}\right)^{1/4}. \tag{7}$$

This estimate is realistic, since disks near their fragmentation threshold are indeed likely to be optically thick (Matzner & Levin 2005, discussion below their Equation (37)), and because viscous heating is minimal beyond a few tens of AU (Kratter et al. 2010b). In our evaluation, we use L_* as calculated in our simulation; although this is somewhat affected by unresolved dynamics through its dependence on the accretion rate, we believe the error to be small. And, since our goal is to evaluate stability in a way that is independent of poorly resolved disk radii, we consider a definite radius–mass relation, $r_{\rm d} = 200(M_*/M_\odot)$ AU. This scaling follows from the assumption that the disk radius scales with the core radius; if cores share a common turbulent Mach number, then their maximum disk size is proportional to $R_{\rm core}$, although there may be large fluctuations around this trend. When cores are pressure confined and supported by both thermal pressure and subsonic turbulence, then core radius, and thus disk radius, scales linearly with mass at fixed temperature. Note that the form of this relation is relatively unimportant as disk stability is determined by the maximum size to which the disk grows (Matzner & Levin 2005). We adjust the normalization of this scaling to match our high-resolution runs. In Figure 9, we plot ξ for each star in the RT run as a function of the star's current mass. For comparison, we also show ξ calculated at a constant radius of 50 AU for one of the stars. The overall variability of ξ is due to variable accretion rates and thus stellar luminosities, while the increase with mass is due primarily to a decrease in temperature as the characteristic radius increases. At low masses, the analytic radii are significantly smaller than those in the simulations, which are somewhat enlarged due to numerical diffusion; in reality disks may be larger and less coherent at early times than analytic models predict. We find that the radius normalization must be increased to at least 600 AU, a very large disk size for these stellar masses, before a significant number of ξ–M values move into the unstable regime. This result is consistent with the global trends of ξ and Γ derived in the previous sections.

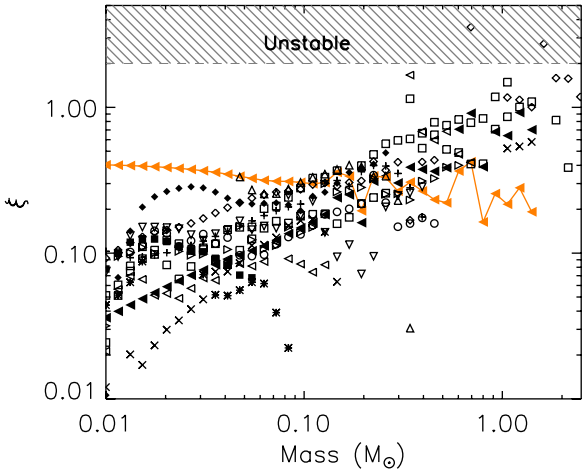

Figure 9. Value of $\xi_{\rm d,ir}$ calculated for the estimated irradiated disk temperature, $T_{\rm d,ir}$, at a mass-dependent radius of $r_{\rm d} = 200(M_*/M_\odot)$ AU for each particle (black). For comparison, we also show the ξ trajectory for one of the particles at a fixed radius of 50 AU (triangles connected with solid, orange line). The hatched region indicates approximate values of ξ at which systems will become unstable for values of $10^{-3} < \Gamma < 5 \times 10^{-2}$.

(A color version of this figure is available in the online journal.)

Stabilization out to such large radii is due to strong external radiation at early times. Otherwise disks become unstable outside of a much smaller radius, within which cooling times are too long and viscous heating alone suffices to suppress fragmentation (Rafikov 2005; Matzner & Levin 2005; Clarke 2009).

5. DISCUSSION

5.1. Sensitivity to Parameter Definitions

We use the parameters ξ and Γ as proxies for gravitational fragmentation but, as we discussed in Section 3.2, our evaluation of these parameters depends somewhat on our ability to discriminate disk from infall. To gauge what uncertainty this may cause, we reevaluate Γ and ξ using $T_{\rm d}$, $\langle j \rangle_{\rm in}$, and $\dot{M}_{\rm in}$ averaged on (or within) a sphere of radius 1000 AU centered on the protostar, well outside the actual disk but close enough that the enclosed mass is dominated by disk material.

Figure 10 shows ξ for the first forming protostar in the RT and RTC simulations with the parameters estimated from the fiducial disk definition and from a sphere with radius 1000 AU. The ξ values for the two different geometries follow a similar progression and they are generally within a factor of 2. This confirms that the accretion rate on small scales is driven by the larger scale characteristics of the core and is not particularly sensitive to the details of the disk geometry or analysis. The difference between the RT and RTC cases is preserved using the spherical geometry and is determined mainly by the different mean temperatures in the two cases (see Section 3).

We find similar agreement between the two methods of evaluation when this analysis is repeated for Γ: the RT rotational parameter in the disk and sphere geometries is within a factor of $\sim$2. The two RTC Γ values follow a similar trend and lie within a factor of 3.

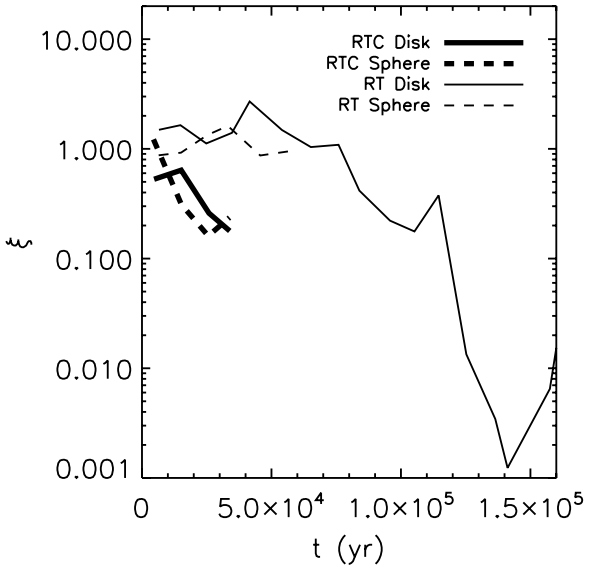

Figure 10. Thermal parameter, ξ, vs. time for the first forming protostar in the RT and RTC (bold) calculations using the fiducial disk definition (solid) and a 1000 AU sphere (dashed).

5.2. Simplifying Assumptions

The caveats of the numerical methods are discussed in detail by OKMK09. We revisit two main caveats here in the context of these results.

Magnetic fields are indisputably important in star formation. Certainly they play a role in launching outflows, which we discuss below, and also serve as a source of pressure that may resist and slow the influence of gravity. Methods using 3D ideal magnetohydrodynamics (MHD) find that the inclusion of magnetic fields suppresses disk fragmentation in the parameter space applicable to low-mass star formation (Price & Bate 2007; Hennebelle & Teyssier 2008), a result that is complementary to the role we find for radiative feedback. These simulations suggest that even the formation of a disk may be suppressed if the field is strong and the angular momentum vector is aligned with the field. However, ideal MHD implicitly overestimates the field strength in collapsing regions by neglecting reconnection and diffusion. Methods that include either ambipolar diffusion or ohmic dissipation, but do not include radiative feedback, find that fragmentation may still occur in disks, particularly if the disk rotation rate is sufficiently high (Machida et al. 2008; Duffin & Pudritz 2009). In sum, magnetic fields most likely reduce disk fragmentation, and since we find no disk fragmentation when radiative feedback is included and both accretion and rotation rates are low, our conclusions would be unchanged.

The greatest uncertainty in our results arises from the absence of protostellar outflows, which impact both the accretion and luminosity. Observations of starless cores indicate that the core mass function shape is similar to the stellar initial mass function but is shifted to higher masses by a factor of 3 (Alves et al. 2007; Enoch et al. 2008). This difference is generally interpreted as an efficiency factor reflecting the amount of gas launched and entrained in outflows (Matzner & McKee 2000), although it does not imply a one-to-one correspondence between cores and stars.

By making some simple assumptions, we can estimate an upper limit on the effect of neglecting outflows. We first adopt a constant efficiency factor, $\epsilon = 1/3$, and assume that the accretion time remains constant (i.e., $M_*/\dot{M}_{\rm in} = $ constant). Under this transformation, a star in the calculation with final mass 1 $M_\odot$ would instead accrete with 0.33 $\dot{M}_{\rm in}$ and have a final mass of 0.33 $M_\odot$. Since accretion dominates the luminosity for most of the simulation (OKMK09), we approximate the total luminosity by

$$L_* \simeq L_{\rm acc} = f_{\rm acc}\frac{GM_*\dot{M}_{\rm in}}{R_*}, \quad (8)$$

where $f_{\rm acc}$ is the fraction of accretion energy that is radiated away and R_* is the protostellar radius. A power-law fit of a one-zone stellar evolution model calibrated to the evolutionary tracks of Hosokawa & Omukai (2009) gives $R_* \propto M_*^{0.3}\dot{M}_{\rm in}^{0.1}$. Altogether, the luminosity varies as $\epsilon^{1.6}$.

From Equation (7), the disk temperature $T_d \propto (\epsilon^{-0.35}L_*/r_{\rm d}^2)^{1/4}$ $\propto \epsilon^{0.89}$, where $\langle j_{\rm in}\rangle$ is roughly independent of ϵ (e.g., Matzner & McKee 2000) and the disk radius in a given core scales inversely with the mass: $r_{\rm d} \propto \langle j_{\rm in}\rangle^2/M_*$. This gives $\xi \propto \epsilon^{-0.34}$ and $\Gamma \propto \epsilon$. Consequently, outflow mass loss shifts the disks toward lower Γ and higher ξ values. For $\epsilon = 1/3$, all but two RT systems stay to the left of the fragmentation line, indicating that most systems remain stable.

If we relax the assumption that the accretion time is constant and instead assume that $\dot{M}_{\rm in}$ is constant (as in the case of a collapsing isothermal sphere), then $\xi \propto \epsilon^{-0.9}$ while Γ is independent of ϵ. Again only two previously stable systems cross the fragmentation line, although several additional systems lie very close to the line. Reducing the core efficiency thus has a mildly destabilizing effect on the disks. These corrected values represent an upper limit on the change in the parameters, so it appears unlikely that including outflows in the simulations will decrease disk stability significantly and lead to increased multiplicity.

We note that additional uncertainty may arise from the geometric aspect of outflow cavities, which could affect the nature of the disk illumination. This caveat is implicit in the use of Equations (5)–(7). It is also possible that the interaction of outflows with nearby filaments and cores will in fact increase the amount of turbulent fragmentation, lower the characteristic protostellar mass (Li et al. 2010; C. Hansen 2010, private communication), and thus reduce the mean luminosity further. Preliminary findings indicate that disk fragmentation remains uncommon in calculations where additional fragmentation is triggered by outflow interactions with turbulent filaments (C. Hansen 2010, private communication). Instead, the amount of turbulent fragmentation is elevated relative to disk fragmentation, which supports our thesis that disk fragmentation around low-mass stars is rare.

5.3. Resolution Limitations

In our calculation, we take a conservative approach to the representation of fragmentation with sink particles. Although *N*-body gravitational interactions between particles may be modeled to subgrid cell accuracy, the gravitational interaction between the gas and the stars is not well modeled when the separations are only a few grid cells (Krumholz et al. 2004). We choose to merge close particles rather than follow poorly resolved interactions of the particles and gas and thus introduce an undetermined amount of error into the gas and particle dynamics. As a result, we forfeit resolution of binary systems with separations less than $\sim$200 AU in the RT and NRT simulations. In the RT case, mergers happen relatively seldom and the particles achieve at least a brown dwarf mass before

merging. These are all included in Figure 2, where their initial pair separations suggest that the formation is real rather than numerical. It is also possible that unresolved fragmentation occurs close to the primary star, although our RTC study suggests that this is unlikely in most cases.

Nonetheless, low-resolution gas fragments may form sink particles that would have become thermally supported or dispersed at higher resolution. This situation is more applicable to the NRT simulations, where demonstrably unstable disks are produced when radiation feedback is absent. Although our sink particle method excludes formation in high-velocity gas, for the NRT run it is likely that some cold fragmentation could be reduced by additional sink criteria for the gravitational potential and gravitational boundedness of clumps (Federrath et al. 2010). The NRTC run does exhibit fragmentation at small scales which may be indicative of an unresolved binary. Thus, our results are qualitatively supported by both higher resolution runs and analysis of Γ–ξ and Q.

5.4. Comparison with Observations and Previous Work

These results affirm previous analytic and numerical work modeling protostellar accretion disks. Our simulation sample is comprised of low-mass stars with accretion rates below that required for disk fragmentation as measured through ξ and Γ. The most massive RT star is $\sim$2.5 $M_{\odot}$, which is marginally in the regime where instability might be expected according to Kratter et al. (2008). However, they find that such a system would likely not become unstable until 0.1–0.2 Myr or later. Lower mass stars are expected to fragment at even later times or not at all, consistent with the small amount of time that the RT stars spend to the right of the fragmentation line. In contrast, the NRT and NRTC cases are highly discrepant with the model predictions. It is clear that radiative heating from the primary stars is a crucial component in simulations.

Most of the core fragmentation occurs around separations of $\sim$0.01–0.02 pc. Observations of dense starless cores in Perseus suggest that the initial density profile is relatively smooth outside the beam resolution of $\sim$1200 AU (Schnee et al. 2010). Two of the 11 cores in the sample are found to have elongation on scales of a few thousand AU that may be indicative of unresolved fragmentation. A very smooth density distribution could preclude wide fragmentation as a means for forming binary systems. However, our turbulence-produced fragments are rare and would be missed at the resolution of Schnee et al. (2010). It is also possible that the observed starless cores may never form protostars or are younger than the objects we focus on in this paper and may undergo fragmentation sometime in the future.

Maury et al. (2010) probe the multiplicity of Class 0 objects with sensitivity down to 50 AU separations. Of the five sources in their sample, only one shows evidence of a companion. This potential binary has a separation of $\sim$1900 AU, which suggests that it did not result from disk fragmentation. Their findings, together with Looney et al. (2000), are consistent with our prediction that low-mass protostars are not members of high-order multiple systems and that any companions mostly likely originate from turbulent core fragmentation and form with a large initial separation.

Low-mass star systems like those modeled here are observed to have a much lower binary fraction than higher mass stars (Lada 2006). In particular, only 30% of M dwarfs, the most common stellar type, have lower mass companions. However, both simulations and analytic work predict that the more massive disks around high-mass stars undergo fragmentation leading to additional stellar companions (Kratter & Matzner 2006; Krumholz et al. 2007). A significant fraction of the difference may be due simply to the absence of disk fragmentation around low-mass stars. OKMK09 report a single star fraction of $0.8+0.2/-0.4$ or 0.5 ± 3 assuming all mergers result instead in a binary. These are likely upper and lower limits, respectively, on the actual single star fraction, since the distribution may evolve over time due to interactions between stars (Duchêne et al. 2007). Although the statistics are poor, these values are consistent with the single star fraction of 0.7 (Lada 2006).

Using the simulations, we can make predictions for the initial range of binary separations. Excluding binaries below the simulation resolution, these are in fact much larger than the typical separation of $\sim$50 AU, although there is a wide distribution around the mean, which varies with stellar mass and possibly from region to region (Duquennoy & Mayor 1991; Fisher 2004); Raghavan et al. (2010) find a Gaussian distribution for periods peaked at $10^{5.03}$ days, implying 48 AU separations for a total system mass of 1.5 $M_{\odot}$. This suggests that significant evolution of the separations must take place after the core fragments. The discrepancy is even larger for very low-mass binaries, whose maximum separations are $1450(M_{\rm tot}/M_{\odot})^2$ AU for systems $\lesssim 0.6\,M_{\odot}$ (Burgasser et al. 2003; Lafrenière et al. 2008), although wide binary exceptions do exist (Radigan et al. 2008, 2009). We favor a scenario in which close low-mass binaries form via interaction with the ongoing infall and between the two accretion disks; loosely bound companions can be stripped by close encounters within the protocluster. (The initial subvirial velocity dispersion of the stars predisposes young clusters to dynamical interactions that will impact the final binary distribution (Bate et al. 2003; Offner et al. 2009a.)

6. CONCLUSIONS

In this work, we revisit the turbulent, self-gravitating radiation-hydrodynamics calculations performed by Offner et al. (2009) in order to characterize the protostellar systems in terms of the thermal parameter, ξ, and the rotational parameter, Γ. We first use high-resolution simulations to confirm the stability criteria derived in KMKK10 under non-turbulent, idealized conditions. The high-resolution simulations further demonstrate that the dimensionless parameters are converged at lower resolution and, thus, they are sufficient to describe the evolutionary state of the protostellar disks even in the case where the scale height and disk structure are not well resolved and where the infall rate is fluctuating and turbulent.

As expected, we find that ξ and Γ are distinct in the cases with and without radiative feedback. In the former case, fragmentation occurs preferentially on scales of $\sim$1000 AU rather than within disks. These two parameters indicate that protostellar accretion disks around low-mass protostars will be stable against gravitational fragmentation for nearly all times. As an independent test, we perform a semi-analytic analysis using the simulated accretion rates and luminosities, which confirms that these disks are stable out to large radii.

Under a scenario of stable accretion disks, low-mass binary systems arise as a result of multiple collapse events in a turbulent core. It follows that the observed multiplicity of low-mass stellar systems arises predominantly due to turbulent fragmentation in the parent core.

We thank the anonymous referee for useful suggestions, which have improved the manuscript. This research has

been supported by the NSF through the grant AST-0901055 (S.S.R.O.). K.M.K. is supported in part by an Ontario Graduate Scholarship. C.D.M. is supported by NSERC and an Ontario Early Researcher Award. R.I.K. is supported by NASA through ATFP grant NNX09AK31G; the NSF through grant AST-0908553 and the US Department of Energy at the Lawrence Livermore National Laboratory under contract DE-AC52-07NA 27344. M.R.K. acknowledges support from: an Alfred P.Sloan Fellowship; NASA through ATFP grant NNX09AK31G; NASA as part of the Spitzer Theoretical Research Program, through a contract issued by the JPL; the National Science Foundation through grant AST-0807739.

REFERENCES

Adams, F. C., Ruden, S. P., & Shu, F. H. 1989, ApJ, 347, 959
Alves, J., Lombardi, M., & Lada, C. J. 2007, A&A, 462, L17
Andre, P., & Montmerle, T. 1994, ApJ, 420, 837
Bate, M. R. 2009, MNRAS, 392, 1363
Bate, M. R., Bonnell, I. A., & Bromm, V. 2003, MNRAS, 339, 577
Bate, M. R., Bonnell, I. A., Clarke, C. J., Lubow, S. H., Ogilvie, G. I., Pringle, J. E., & Tout, C. A. 2000, MNRAS, 317, 773
Boley, A. C., Durisen, R. H., Nordlund, Å., & Lord, J. 2007, ApJ, 665, 1254
Bonnell, I. A., & Bate, M. R. 1994, MNRAS, 269, L45
Burgasser, A. J., Kirkpatrick, J. D., Reid, I. N., Brown, M. E., Miskey, C. L., & Gizis, J. E. 2003, ApJ, 586, 512
Cai, K., Durisen, R. H., Boley, A. C., Pickett, M. K., & Mejía, A. C. 2008, ApJ, 673, 1138
Clarke, C. J. 2009, MNRAS, 396, 1066
Duchêne, G., Delgado-Donate, E., Haisch, K. E., Jr., Loinard, L., & Rodríguez, L. F. 2007, in Protostars and Planets V, ed. B. Reipurth, D. Jewitt, & K. Keil (Tucson, AZ: Univ. Arizona Press), 379
Duffin, D. F., & Pudritz, R. E. 2009, ApJ, 706, L46
Duquennoy, A., & Mayor, M. 1991, A&A, 248, 485
Enoch, M. L., Evans, N. J., Sargent, A. I., II, Glenn, J., Rosolowsky, E., & Myers, P. 2008, ApJ, 684, 1240
Evans, N. J., et al. 2009, ApJS, 181, 321
Federrath, C., Banerjee, R., Clark, P. C., & Klessen, R. S. 2010, ApJ, 713, 269
Fisher, R. T. 2004, ApJ, 600, 769
Foster, P. N., & Chevalier, R. A. 1993, ApJ, 416, 303
Gammie, C. F. 2001, ApJ, 553, 174
Goldreich, P., & Lynden-Bell, D. 1965, MNRAS, 130, 125
Goodwin, S. P., Kroupa, P., Goodman, A., & Burkert, A. 2007, in Protostars and Planets V, ed. B. Reipurth, D. Jewitt, & K. Keil (Tucson, AZ: Univ. Arizona Press), 133
Goodwin, S. P., Whitworth, A. P., & Ward-Thompson, D. 2004, A&A, 414, 633
Hale, A. 1994, AJ, 107, 306
Hennebelle, P., & Teyssier, R. 2008, A&A, 477, 25
Hosokawa, T., & Omukai, K. 2009, ApJ, 691, 823
Howe, K. S., & Clarke, C. J. 2009, MNRAS, 392, 448
Jensen, E. L. N., Mathieu, R. D., Donar, A. X., & Dullighan, A. 2004, ApJ, 600, 789
Klessen, R. S., & Burkert, A. 2000, ApJS, 128, 287
Kratter, K. M., & Matzner, C. D. 2006, MNRAS, 373, 1563
Kratter, K. M., Matzner, C. D., & Krumholz, M. R. 2008, ApJ, 681, 375
Kratter, K. M., Matzner, C. D., Krumholz, M. R., & Klein, R. I. 2010a, ApJ, 708, 1585
Kratter, K. M., Murray-Clay, R. A., & Youdin, A. N. 2010b, ApJ, 710, 1375
Krumholz, M. R., Klein, R. I., & McKee, C. F. 2007, ApJ, 656, 959
Krumholz, M. R., McKee, C. F., & Klein, R. I. 2004, ApJ, 611, 399
Lada, C. J. 2006, ApJ, 640, L63
Lafrenière, D., Jayawardhana, R., Brandeker, A., Ahmic, M., & van Kerkwijk, M. H. 2008, ApJ, 683, 844
Li, Z., Wang, P., Abel, T., & Nakamura, F. 2010, ApJ, 720, L26
Looney, L. W., Mundy, L. G., & Welch, W. J. 2000, ApJ, 529, 477
Lubow, S. H., & Ogilvie, G. I. 2000, ApJ, 538, 326
Machida, M. N., Tomisaka, K., Matsumoto, T., & Inutsuka, S. 2008, ApJ, 677, 327
Matzner, C. D., & Levin, Y. 2005, ApJ, 628, 817
Matzner, C. D., & McKee, C. F. 2000, ApJ, 545, 364
Maury, A. J., et al. 2010, A&A, 512, A40
Melo, C. H. F., Covino, E., Alcalá, J. M., & Torres, G. 2001, A&A, 378, 898
Mitchell, J. 1767, Phil. Trans. R. Soc., 76, 97
Monin, J., Ménard, F., & Peretto, N. 2006, A&A, 446, 201
Nelson, A. F. 2006, MNRAS, 373, 1039
Offner, S. S. R., Hansen, C. E., & Krumholz, M. R. 2009a, ApJ, 704, L124
Offner, S. S. R., Klein, R. I., & McKee, C. F. 2008, ApJ, 686, 1174
Offner, S. S. R., Klein, R. I., McKee, C. F., & Krumholz, M. R. 2009b, ApJ, 703, 131
Price, D. J., & Bate, M. R. 2007, MNRAS, 377, 77
Radigan, J., Lafrenière, D., Jayawardhana, R., & Doyon, R. 2008, ApJ, 689, 471
Radigan, J., Lafrenière, D., Jayawardhana, R., & Doyon, R. 2009, ApJ, 698, 405
Rafikov, R. R. 2005, ApJ, 621, L69
Raghavan, D., et al. 2010, ApJS, 190, 1
Schnee, S., Enoch, M., Johnstone, D., Culverhouse, T., Leitch, E., Marrone, D., & Sargent, A. 2010, ApJ, 718, 306
Scholz, A., et al. 2010, MNRAS, in press
Sellwood, J. A., & Carlberg, R. G. 1984, ApJ, 282, 61
Shakura, N. I., & Sunyaev, R. A. 1973, A&A, 24, 337
Shu, F. H. 1977, ApJ, 214, 488
Shu, F. H., Tremaine, S., Adams, F. C., & Ruden, S. P. 1990, ApJ, 358, 495
Stamatellos, D., & Whitworth, A. P. 2009, MNRAS, 392, 413
Stone, J. M., Ostriker, E. C., & Gammie, C. F. 1998, ApJ, 508, L99
Tohline, J. E. 2002, ARA&A, 40, 349
Toomre, A. 1964, ApJ, 139, 1217
Truelove, J. K., Klein, R. I., McKee, C. F., Holliman, J. H., II, Howell, L. H., & Greenough, J. A. 1997, ApJ, 489, L179
Walch, S., Burkert, A., Whitworth, A., Naab, T., & Gritschneder, M. 2009, MNRAS, 400, 13
White, R. J., & Hillenbrand, L. A. 2004, ApJ, 616, 998